












RESEARCH ARTICLE

Elevated photic response is followed by a rapid decay and depressed state in ictogenic networks

Sverre Myren-Svelstad^{1,2,3}  | Ahmed Jamali^{1,2,3}  | Sunniva S. Ophus¹  | Percival P. D'gama^{1,4}  | Anna M. Ostenrath¹  | Aytac Kadir Mutlu¹  | Helene Homme Hoffshagen¹  | Adriana L. Hotz⁵  | Stephan C. F. Neuhauss⁵  | Nathalie Jurisch-Yaksi^{1,3,4}  | Emre Yaksi^{1,6} 

¹Kavli Institute for Systems Neuroscience and Centre for Neural Computation, Faculty of Medicine and Health Sciences, Norwegian University of Science and Technology, Trondheim, Norway

²Department of Neuromedicine and Movement Science, Faculty of Medicine and Health Sciences, Norwegian University of Science and Technology, Trondheim, Norway

³Department of Neurology and Clinical Neurophysiology, St Olav's University Hospital, Trondheim, Norway

⁴Department of Clinical and Molecular Medicine, Faculty of Medicine and Health Sciences, Norwegian University of Science and Technology, Trondheim, Norway

⁵Department of Molecular Life Sciences, University of Zürich, Zürich, Switzerland

⁶Koç University Research Center for Translational Medicine, Department of Neurology, Koç University School of Medicine, Istanbul, Turkey

Correspondence

Emre Yaksi, Olav Kyrres Gate 9, 7030 Trondheim, Norway.

Email: emre.yaksi@ntnu.no

Nathalie Jurisch-Yaksi, Erling Skjalgssons Gate 1, 7030 Trondheim, Norway.

Email: nathalie.jurisch-yaksi@ntnu.no

Funding information

H2020 European Research Council, Grant/Award Number: 335561; Helse Midt-Norge, Grant/Award Number: 90158500; Norges Forskningsråd, Grant/Award Number: 239973 and 314189

Abstract

Objective: The switch between nonseizure and seizure states involves profound alterations in network excitability and synchrony. In this study, we aimed to identify and compare features of neural excitability and dynamics across multiple zebrafish seizure and epilepsy models.

Methods: Inspired by video-electroencephalographic recordings in patients, we developed a framework to study spontaneous and photically evoked neural and locomotor activity in zebrafish larvae, by combining high-throughput behavioral tracking and whole-brain in vivo two-photon calcium imaging.

Results: Our setup allowed us to dissect behavioral and physiological features that are divergent or convergent across multiple models. We observed that spontaneous locomotor and neural activity exhibit great diversity across models. Nonetheless, during photic stimulation, hyperexcitability and rapid response dynamics were well conserved across multiple models, highlighting the reliability of photically evoked activity for high-throughput assays. Intriguingly, in several models, we observed that the initial elevated photic response is often followed by rapid decay of neural activity and a prominent depressed state. Elevated photic response and following depressed state in seizure-prone networks are significantly

Sverre Myren-Svelstad and Ahmed Jamali contributed equally to this work. Emre Yaksi and Nathalie Jurisch-Yaksi jointly supervised this work.

This is an open access article under the terms of the [Creative Commons Attribution-NonCommercial-NoDerivs](https://creativecommons.org/licenses/by-nc-nd/4.0/) License, which permits use and distribution in any medium, provided the original work is properly cited, the use is non-commercial and no modifications or adaptations are made.

© 2022 The Authors. *Epilepsia* published by Wiley Periodicals LLC on behalf of International League Against Epilepsy.

reduced by the antiseizure medication valproic acid. Finally, rapid decay and depression of neural activity following photic stimulation temporally overlap with slow recruitment of astroglial calcium signals that are enhanced in seizure-prone networks.

Significance: We argue that fast decay of neural activity and depressed states following photic response are likely due to homeostatic mechanisms triggered by excessive neural activity. An improved understanding of the interplay between elevated and depressed excitability states might suggest tailored epilepsy therapies.

KEYWORDS

astroglia, calcium imaging, depressed state, elevated state, epilepsy, high-throughput behavior, hyperexcitability, photic stimulation, seizure, zebrafish

1 | INTRODUCTION

Epilepsy is one of the most dynamic brain disorders. The switch between nonseizure and seizure states involves profound alterations in network excitability and synchrony. Increased excitability is often considered to be the main seizure generating mechanism,^{1,2} and many antiseizure drugs act by preventing hyperexcitable states.³ Strikingly, decreased excitability is also observed during seizure generation (ictogenesis). For example, hypoactivity of cholinergic neurons in brainstem nuclei and basal forebrain is proposed to induce impaired consciousness in temporal lobe seizures.^{4,5} Moreover, enhanced γ -aminobutyric acidergic (GABAergic) inhibition of thalamocortical neurons may underlie absence seizures.⁶ A widespread and transient hypoactivity is the hallmark of post-tonic-clonic seizure states.⁷ Consequently, spreading of hypoexcitability across local and global networks may explain important seizure symptoms. Despite such intriguing observations from animal studies and human patients, the interplay between hyperexcitable and hypoexcitable states in ictogenic networks remains poorly understood.

Clinical and fundamental applications of systems neuroscience are currently boosting our understanding of epilepsy as a network disorder.^{8–11} Recording whole-brain activity with high spatiotemporal resolution, however, is challenging in human patients and rodent models due to anatomical and technical constraints. Here, we performed *in vivo* two-photon calcium imaging across the entire brain of small and transparent zebrafish larvae, to explore the dynamics of altered network excitability.^{12–15} Inspired by video-electroencephalography (video-EEG) and photic stimulation protocols that are commonly used in human patients, we performed complementary recordings of

Key Points

- Features of spontaneous locomotor and neural activity vary across zebrafish seizure and epilepsy models
- We propose that photic stimulation may serve as a useful tool to investigate behavioral and neurophysiological phenotypes in zebrafish seizure and epilepsy models
- We observed elevated activity with faster dynamics in response to photic stimulation in all tested zebrafish models
- Photically evoked neural responses were often followed by a depressed state, which temporally overlaps with slow recruitment of astroglial calcium signals that are enhanced in seizure-prone networks

animal behavior and whole-brain activity.¹⁶ We delivered photic stimulation to trigger neural responses, because photosensitivity is an important physiological trait in epilepsy.^{16–20} Spontaneous locomotor and neural activity displayed a hypoactive or hyperactive phenotype depending on the seizure or epilepsy model.^{15,21–26} Photic stimulation evoked increased swim velocities and change in swim angle, in line with tonic-clonic seizure-like behavior observed in zebrafish larvae.²² Intriguingly, photic stimuli induced striking neural dynamics, where an elevated state often was followed by a prominent depressed state. Both elevated and depressed states are reduced by a common antiseizure drug, valproic acid (VPA). Pentylentetrazole (PTZ), a proconvulsive GABA_A antagonist,^{15,22,23} elicited dose-dependent elevated-to-depressed network responses, which were

not observed in control animals. The *gabra1* knockout model of the $\alpha 1$ subunit of GABA_A receptor²⁶ resembled low-dose PTZ dynamics. A genetic model with a dissimilar pathophysiology, the *eaat2a* knockout model lacking the major astroglial glutamate transporter^{25,27} exhibited elevated photic responses followed by less pronounced depressed states. To gain further insights into the mechanisms involved in the depressed states, we imaged astroglial calcium activity in the pharmacological PTZ model. We observed highly elevated astroglial calcium signals, which were anticorrelated with neural activity during depressed state, suggesting that astroglial networks are involved in this depression phase. Taken together, we show that the brain networks' adaptation to photic stimulation involves dynamic and rapid switching between elevated and depressed states.

2 | MATERIALS AND METHODS

2.1 | Contact for reagent and resource sharing

Further information and requests for reagents may be directed to and will be fulfilled by the lead author Emre Yaksi (emre.yaksi@ntnu.no).

2.2 | Experimental model and subject details

2.2.1 | Fish maintenance

Fish were kept in 3.5-L tanks at a density of 15–20 fish per tank in a Techniplast Multilinking system at temperature 28°C, pH 7, O₂ 6.0 ppm, 700 μ S, on a 14:10 hour light/dark cycle. Fish received dry food (Zebrafeed, Sparos I&D Nutrition in Aquaculture) two times per day and *Artemia nauplii* once per day (Grade 0, Argent Laboratories). Larvae were maintained in egg water (1.2 g marine salt, 20 L reverse osmosis [RO] water, 1:1000 .1% methylene blue) from fertilization to 3 days postfertilization (dpf) and in artificial fish water (AFW; 1.2 g marine salt in 20 L RO water) from 3 to 5 dpf. The animal facilities were approved by the Norwegian Food Safety Authority (NFSA). All experimental procedures were performed on zebrafish larvae up to 5 dpf and in accordance with the directive 2010/63/EU of the European Parliament and the NFSA.

For experiments, the following fish lines were used: *Tg(elavl3:GCaMP6s)*,^{15,28} *Tg(GFAP:Gal4)nw7*,¹⁵ *Tg(UAS:GCaMP6s)*,²⁹ *eaat2a*,²⁵ *gabra1^{udm103}*,²⁶ *scn1lab^{s55221}*,²¹ and wild-type.

2.2.2 | Behavior tracking and experimental design

Behavior tracking was performed on 5 dpf wild-type ($n = 216$ for 3-h, $n = 168$ for 1-h PTZ experiments; $n = 88$ for 1-h PTZ + VPA experiments), *gabra1* ($n = 168$), *eaat2a* ($n = 120$), and *scn1lab* ($n = 264$) larvae. We used a commercially available automated tracking system (Zantiks), which has built-in tracking software and control of light stimuli. Animals were placed in a 24-well plate (VWR, Avantor). For the PTZ experiments, wells were filled with 2 ml of PTZ or AFW. For the PTZ + VPA experiments, larvae were preincubated with 5 mmol·L⁻¹ VPA for 1 h³⁰ and the VPA treatment was continued throughout the experiment. For the other experiments, all wells were filled with 2 ml AFW. Fish were placed into the wells immediately before the start of the experiments. After 1 h of acclimatization, the lights were turned off for 10 min, followed by “white” light stimulation of 10 s applied with interstimulus intervals (ISIs) of 10, 5, 2, and 1 min, with five repetitions for each ISI. Total recording duration was 3 h. In the PTZ model, we additionally did 1-h recordings of 10-min baseline (in darkness), followed by 10-s light stimuli with ISIs of 5, 2, 1, .5, and .25 min, with five repetitions for each ISI.

2.2.3 | Two-photon calcium imaging

Two-photon calcium imaging was performed on 5 dpf *Tg(elavl3:GCaMP6s)* ($n = 41$ for PTZ experiments, $n = 9$ for PTZ + VPA experiments), *Tg(GFAP:Gal4)nw7;Tg(UAS:GCaMP6s)* ($n = 16$ for PTZ experiments), *gabra1;Tg(elavl3:GCaMP6s)* ($n = 31$), and *eaat2a;Tg(elavl3:GCaMP6s)* ($n = 38$) zebrafish larvae. Animals were paralyzed upon injection of α -bungarotoxin (Invitrogen B1601, 1 mg/ml)^{15,31} and embedded in 1.5% low melting point agarose in recording chambers (Fluorodish, World Precision Instruments). After 10 min of agarose solidification, either .75 ml (for PTZ experiments) or 1.5 ml (for the genetic models) AFW was added on top of the agarose. Immediately before the start of PTZ experiments, PTZ solution was added for final concentrations of 1, 5, or 15 mmol·L⁻¹. For the PTZ + VPA experiments, larvae were preincubated with 5 mmol·L⁻¹ VPA for 1 h³⁰ and the treatment was continued throughout the experiment. The recordings were performed in a two-photon microscope (Scientifica) using a 16 \times water immersion objective (Nikon, numerical aperture = .8, Long Working Distance 3.0, plan) and a Ti:Sapphire laser (MaiTai Spectra-Physics) tuned at 920 nm. Recordings of 1536 \times 650 pixels were acquired at a rate of 2.43 Hz. A subset of the recordings were acquired at a rate of 24.3 Hz and downsampled to

2.43 Hz before analysis. Spontaneous calcium activity was recorded for 10 min in darkness, followed by stimuli of 10 s using a red light-emitting diode light (LZ1-00R105, LedEngin; 625 nm),³² five repetitions each for ISIs of 5, 2, 1, .5, and .25 min. Total recording duration was 60 min. Animals without cerebral blood flow after the experiments were excluded.

2.2.4 | Genotyping

For *eaat2a* and *gabra1* lines, genotypes were determined by real-time quantitative polymerase chain reaction melt-curve analyses.^{25,26} For *scn1lab*, KASP assay (LGC Biosearch Technologies) was performed.³³

2.2.5 | Data analysis

Behavioral data from the tracking system was retrieved as position over time, and analyzed by custom-made MATLAB scripts. Periods with extreme swim velocities above the 99.96th percentile of the pooled velocities were flagged as possible tracking errors. Subsequently, videos of the experiments with flagged time periods were visually assessed and fish with tracking errors were excluded.

Spontaneous behavioral activity was assessed as the mean velocity over the baseline period (1 h). The velocities were compared within subgroups of each model using Wilcoxon rank-sum test. To calculate mean photically evoked swim velocity, responses from 5-min ISIs were averaged. To compute light-on and light-off peak amplitudes, we found the maximum change in velocity during the first 5 s after lights on and lights off, respectively. To calculate change in swim angle, three subsequent points of the tracking were used to define two vectors. The determinant and the scalar product of the vectors were calculated. Subsequently, the angle was determined as the absolute value of the arctangent of the determinant and the dot product.

Two-photon microscopy images were aligned using a previously reported algorithm.^{31,32} Regions of interest (ROIs) were manually drawn based on anatomical landmarks. For *Tg(elavl3:GCaMP6s)* fish, ROIs were drawn around the telencephalon, thalamus, optic tectum, cerebellum, and brainstem. For *Tg(GFAP:Gal4)nw7;Tg(UAS:GCaMP6s)* larvae, ROIs were drawn around the medial regions surrounding the brain ventricles near the cell bodies of astroglia. For each ROI, the relative change in fluorescence was calculated.³⁴ For spontaneous activity, the last 2 min of the 1-h recording was selected for calculation. The 5 s of fluorescence preceding the stimuli was used as baseline for the calculations of photic responses. Sixty seconds baseline was used for calculation of elevated

and depressed state. Elevated state was calculated as the area under the curve (1-min period from light onset) > 2 SD from this baseline, and depressed state as the area over the curve (2 min from light offset) < 2 SD from baseline. These calculations were performed in MATLAB using the “trapz” function. Linear regression of elevated versus depressed state was calculated using the “fitlm” function.

2.3 | Quantification and statistical analysis

Statistical analysis was done using MATLAB. Wilcoxon rank-sum test was used for nonpaired analysis. Probability of $p < .05$ was considered statistically significant.

2.4 | Data and code availability

The datasets and the codes supporting the current study have not been deposited in a public repository but are available from the corresponding author upon request.

3 | RESULTS

3.1 | Spontaneous locomotor and neural activity display a hypoactive or hyperactive phenotype depending on the seizure or epilepsy model

To investigate excitability in seizure and epilepsy models, we performed locomotor tracking and two-photon calcium imaging in parallel experiments. A tonic-clonic-like seizure phenotype in zebrafish larvae consists of high-speed swirllike swimming followed by a period of immobility.²² Application of the proconvulsant PTZ, a GABA_A antagonist, at high dosage (15 mmol·L⁻¹) led to a significant increase in mean swim speed (Figure 1A, left panel) and change in swim angle (Figure S1, left panel). In *gabra1* mutants with knockout of GABA_A receptor $\alpha 1$ subunits, swim activity and change in swim angle were not altered (Figure 1A, Figure S1, center panels). Strikingly, *eaat2a* mutants lacking the major astroglial glutamate transporter were inactive at baseline, measured by mean swim velocity and change in swim angle (Figure 1A, Figure S1, right panels).²⁵ In the *scn1lab* knockout model of $\alpha 1$ subunit of Na_v1.1 receptors,^{21,24,35,36} the mean swim velocity and mean change in swim angle were significantly lower compared to controls (Figure S2a,f).

Next, we examined the neural activity by two-photon microscopy in *Tg(elavl3:GCaMP6s)* zebrafish larvae expressing calcium indicator *GCaMP6s* in all neurons. We analyzed calcium fluctuations (SD) during baseline.²⁵ The

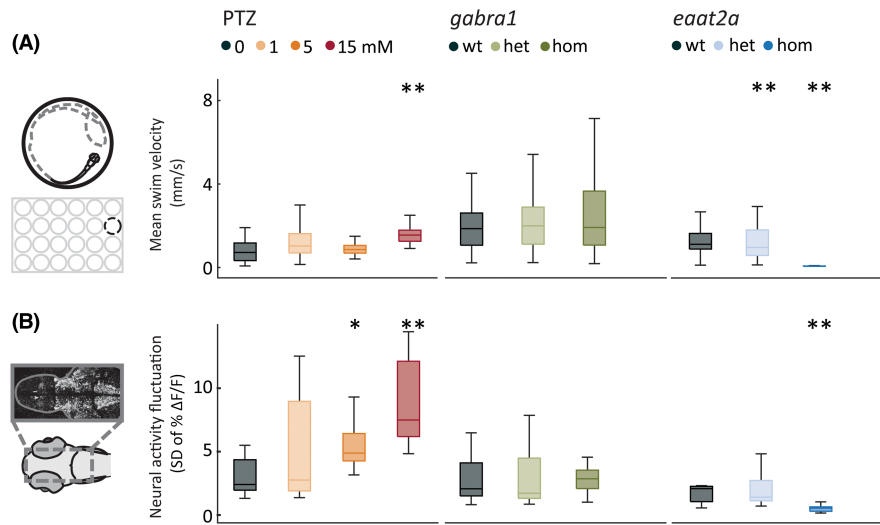


FIGURE 1 Spontaneous locomotor and neural activity display a hypoactive or hyperactive model-dependent phenotype. (A) Locomotor behavior was recorded in a 24-well plate. Mean swim velocity was calculated per 1-s time bin during 1-h baseline recordings in the pentylenetetrazole (PTZ), *gabra1*, and *eaat2a* models. (B) Neural activity fluctuation was calculated as the SD of relative change in fluorescence ($\Delta F/F$; %) during the last 2 min of 1-h recordings in 5-day-old *Tg(elavl3:GCaMP6s)* zebrafish larvae. Total sample size for behavioral experiments for PTZ model: control, $n = 48$; 1 $\text{mmol}\cdot\text{L}^{-1}$, $n = 48$; 5 $\text{mmol}\cdot\text{L}^{-1}$, $n = 48$; 15 $\text{mmol}\cdot\text{L}^{-1}$, $n = 48$; for *gabra1* model: wild-type (wt), $n = 39$; heterozygous (het), $n = 81$; homozygous (hom), $n = 48$; for *eaat2a* model: wt, $n = 11$; het, $n = 41$; hom, $n = 42$. Total sample size for calcium recordings for PTZ model: control, $n = 8$; 1 $\text{mmol}\cdot\text{L}^{-1}$, $n = 7$; 5 $\text{mmol}\cdot\text{L}^{-1}$, $n = 9$; 15 $\text{mmol}\cdot\text{L}^{-1}$, $n = 10$; for *gabra1* model: wt, $n = 9$; het, $n = 13$; hom, $n = 9$; for *eaat2a* model: wt, $n = 7$; het, $n = 13$; hom, $n = 11$. * $p < .05$, ** $p < .01$ by Wilcoxon rank-sum test. Boxplots represent median with interquartile ranges; whiskers extend to the most extreme data points that are not outliers

baseline neural activity resembled locomotor behavior in the PTZ, *gabra1*, and *eaat2a* models (Figure 1B). PTZ application led to a dose-dependent increase in calcium fluctuations (Figure 1B, left panel), in line with increased mean swim velocities. In *gabra1* homozygous larvae, baseline neural activity was not changed (Figure 1B, center panel), whereas homozygous *eaat2a* animals displayed a significant decrease in baseline neural activity (Figure 1B, right panel).²⁵ Two-photon calcium imaging in the *scn1lab* mutants was not possible due to mutation-linked hyperpigmentation. Taken together, our findings reveal that the spontaneous locomotor and neural activity of seizure and epilepsy models may exhibit fundamentally different features ranging from hypo- to hyperactivity. This underlines that a simplistic readout of epilepsy phenotype purely based on altered spontaneous activity or locomotion may not encompass the whole pathophysiology of epilepsy.

3.2 | Photic stimulation leads to model-dependent change in swim velocity and angle

The occurrence of spontaneous seizures is unpredictable. To assess neural hyperexcitability with a better temporal control, we used 10-s photic stimulation with 5-min ISIs. Pharmacological perturbations with PTZ demonstrated distinct locomotor signatures. We found that the

light-on responses were increased for all PTZ concentrations compared to control, with the medium concentration (5 $\text{mmol}\cdot\text{L}^{-1}$) eliciting the strongest mean response (Figure 2A–C, left panels). We also observed stronger light-off responses in PTZ-treated animals (Figure 2D, left panel). Because previous studies reported swirllike zebrafish swim patterns during seizures,²² we next quantified change in swim angle. Change in swim angle was the largest at higher PTZ dosages (Figure 3A–D, left panels). *gabra1* homozygous mutants were similar to higher dose PTZ. The amplitudes of light-on and light-off swim velocity responses were higher (Figure 2A–D, center panels), but the change in swim angle was not significantly different from controls (Figure 3A–D, center panels). The *eaat2a* homozygous larvae had lower amplitudes during both light-on and light-off responses (Figure 2A–D, right panels). Swim angle was not altered in *eaat2a* mutants compared to controls (Figure 3A–D, right panels). In the *scn1lab* homozygous animals, we observed an increased swim velocity and change in angle upon light-on compared to wild-type, whereas light-off amplitudes were unaltered (Figure S2b–e,g–j). Taken together, our results using photic stimulation show that photically evoked swim velocity and change in swim angle are model-dependent.

To test how antiseizure medications alter the behavioral responses to photic stimulation, we compared photic responses of zebrafish larvae exposed to PTZ with the responses to concomitant treatment with PTZ and

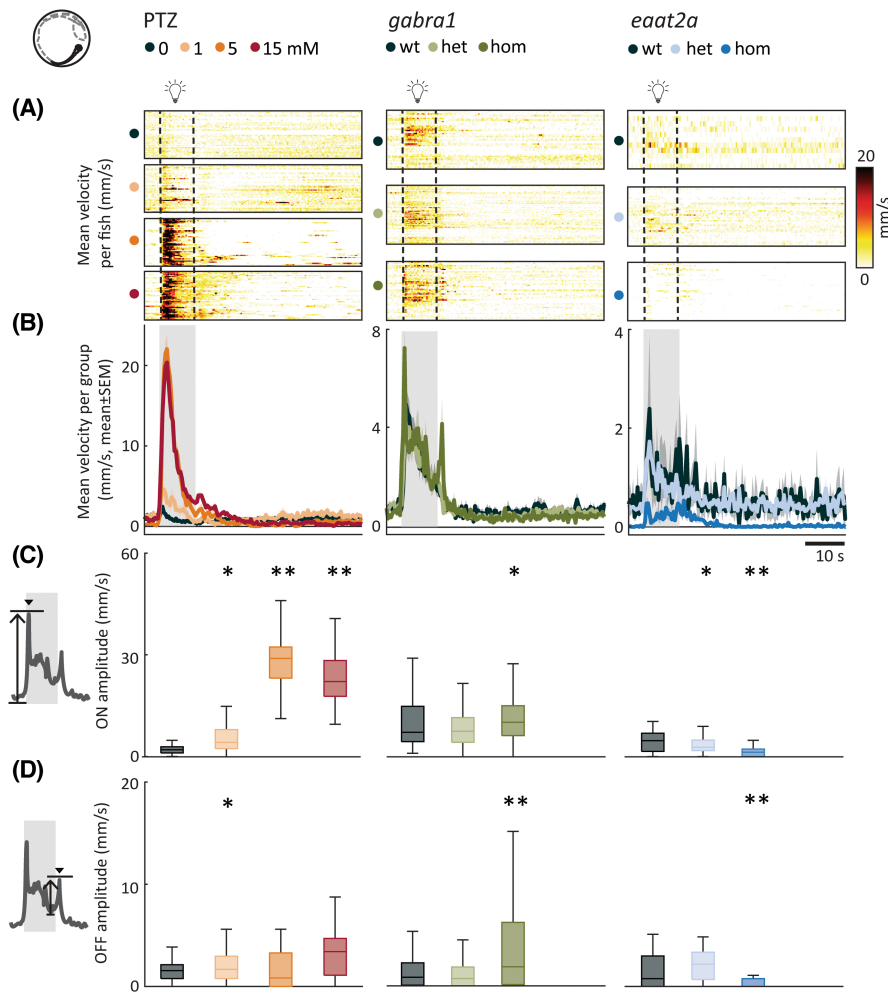


FIGURE 2 Photic stimulation leads to model-dependent change in swim velocity. (A) Mean swim velocity in response to 10-s photic stimulation with 5-min interstimulus interval. Each line in heatmaps represents the average across five trials for one fish. Dashed lines indicate the start and end of photic stimulation. (B) Mean swim velocity per subgroup. Gray shaded area indicates photic stimulation. (C) Light-on amplitude measured as maximum change in velocity during the first 5 s after light onset. (D) Light-off amplitude measured as the maximum change in velocity during the first 5 s after light offset. Total sample size for pentylentetrazole (PTZ) model: control, $n = 42$; $1 \text{ mmol}\cdot\text{L}^{-1}$, $n = 42$; $5 \text{ mmol}\cdot\text{L}^{-1}$, $n = 41$; $15 \text{ mmol}\cdot\text{L}^{-1}$, $n = 41$; for *gabra1* model: wild-type (wt), $n = 39$; heterozygous (het), $n = 81$; homozygous (hom), $n = 48$; for *eaat2a* model: wt, $n = 11$; het, $n = 41$; hom, $n = 42$. * $p < .05$, ** $p < .01$ by Wilcoxon rank-sum test. Shaded regions associated with individual colors represent SEM of each group. Boxplots represent median with interquartile ranges; whiskers extend to the most extreme data points that are not outliers

VPA. Compared to the PTZ group, the zebrafish larvae treated with VPA + PTZ significantly reduced their photically evoked change in swim speed and swim angle (Figure S3a-f). This finding further highlights the potential of photic stimulation as a discovery platform for antiseizure drugs.

3.3 | Fast dynamics of neural activity and prominent depressed network state are observed following photic stimulation

Next, we studied the amplitude and dynamics of neural responses across the brain upon 10-s photic stimulation

with various ISIs. We calculated the mean photically evoked neural calcium signals across trials. For the 5-min ISI in the PTZ model, photic responses had significantly shorter latency to peak ($5 \text{ mmol}\cdot\text{L}^{-1}$; Figure 4A,B, left panel) and higher amplitude (1 and $15 \text{ mmol}\cdot\text{L}^{-1}$) compared to controls (Figure 4C, left panel). Treatment of zebrafish larvae with VPA reduced the amplitude of neural responses to photic stimulation in PTZ-treated zebrafish (Figure S3g,h). In homozygous *gabra1* mutants, the latency of neural response to photic stimulation was significantly shorter than controls, but the amplitude was similar (Figure 4A-C, center panels). In homozygous *eaat2a* larvae, latency was unaltered, but the amplitude was higher (Figure 4A-C, right panels).

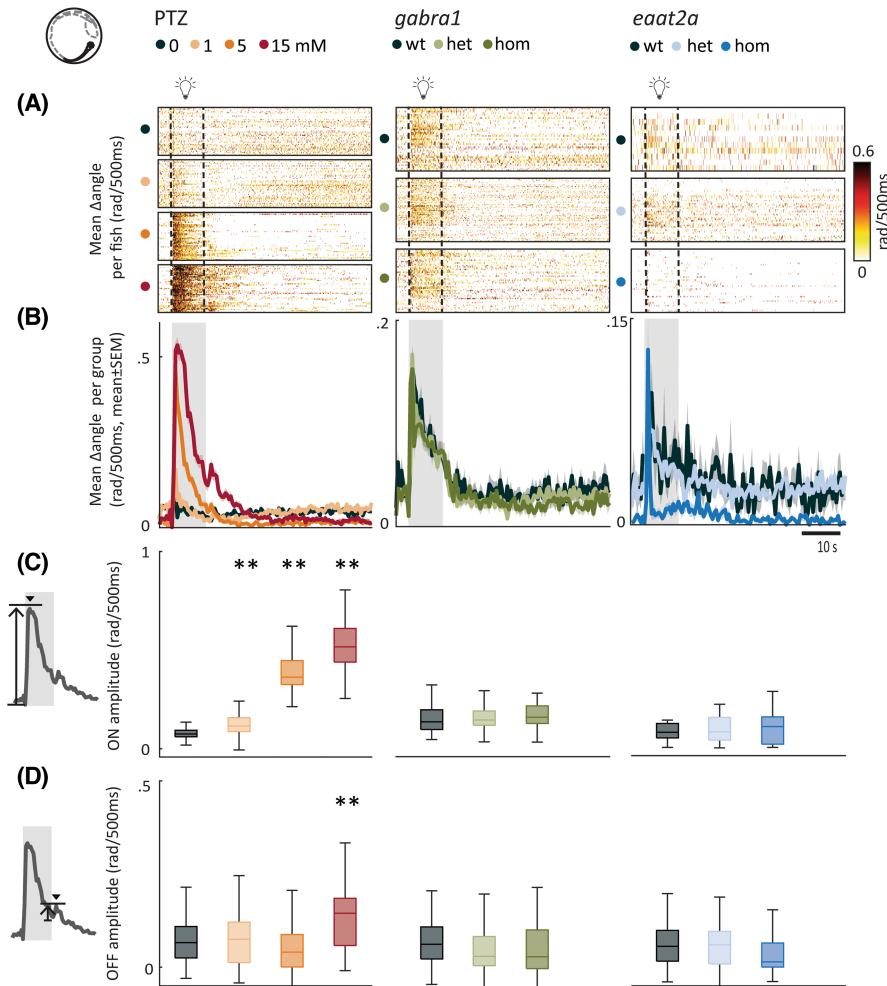


FIGURE 3 Photic stimulation leads to model-dependent change in swim angle. (A) Mean change in swim angle in response to 10-s photic stimulation with 5-min interstimulus interval. Each line in heatmaps represents the average across five trials for one fish. Dashed lines indicate the start and end of 10-s photic stimulation. (B) Mean change in swim angle per subgroup. Gray shaded area indicates photic stimulation. (C) Light-on amplitude measured as maximum change in swim angle during first 5 s after light onset. (D) Light-off amplitude measured as the maximum change in swim angle during the first 5 s after light offset. Total sample size for pentylenetetrazole (PTZ) model: control, $n = 42$; $1 \text{ mmol}\cdot\text{L}^{-1}$, $n = 42$; $5 \text{ mmol}\cdot\text{L}^{-1}$, $n = 41$; $15 \text{ mmol}\cdot\text{L}^{-1}$, $n = 41$; for *gabra1* model: wild-type (wt), $n = 39$; heterozygous (het), $n = 81$; homozygous (hom), $n = 48$; for *eaat2a* model: wt, $n = 11$; het, $n = 41$; hom, $n = 42$. ** $p < .01$ by Wilcoxon rank-sum test. Shaded regions associated with individual colors represent SEM of each group. Boxplots represent median with interquartile ranges; whiskers extend to the most extreme data points that are not outliers

When analyzing dynamics of photically evoked neural activity, we observed a striking phenomenon; the elevated state was followed by a fast decay and subsequent depressed state (Figure 4A, Videos S1–S3). To quantify how fast the elevated state decays into a depressed state, we calculated the decay-time constant from the maximum point of the light-off peak. We observed that this faster decay of neural activity is a feature that was preserved across PTZ concentrations, as well as *gabra1* and *eaat2a* models. For 5-min ISI, the differences between control and 5 or $15 \text{ mmol}\cdot\text{L}^{-1}$ PTZ and for homozygous *eaat2a* were significant, whereas it was not significant for *gabra1* homozygous mutants (Figure 4D). Differences were generally significant for shorter ISIs for PTZ, *gabra1*, and

eaat2a models (Figure S4). This highlights the presence of homeostatic mechanisms that are recruited in response to elevated neural activity and rapidly reduce it to a less excitable or depressed state.

Next, we quantified these elevated and depressed states by calculating the area under the curve (1-min period from light onset) and the area over the curve (2-min period from light offset), respectively. In the $15 \text{ mmol}\cdot\text{L}^{-1}$ PTZ model, elevated and depressed states were correlated (Figure S5), and significantly more prominent compared to controls (Figure 4E,F, left panels). VPA treatment reduced both the elevated and depressed states (Figure S3i,j). For the *gabra1* homozygous larvae, the elevated and depressed states were comparable to controls (Figure 4E,F, center

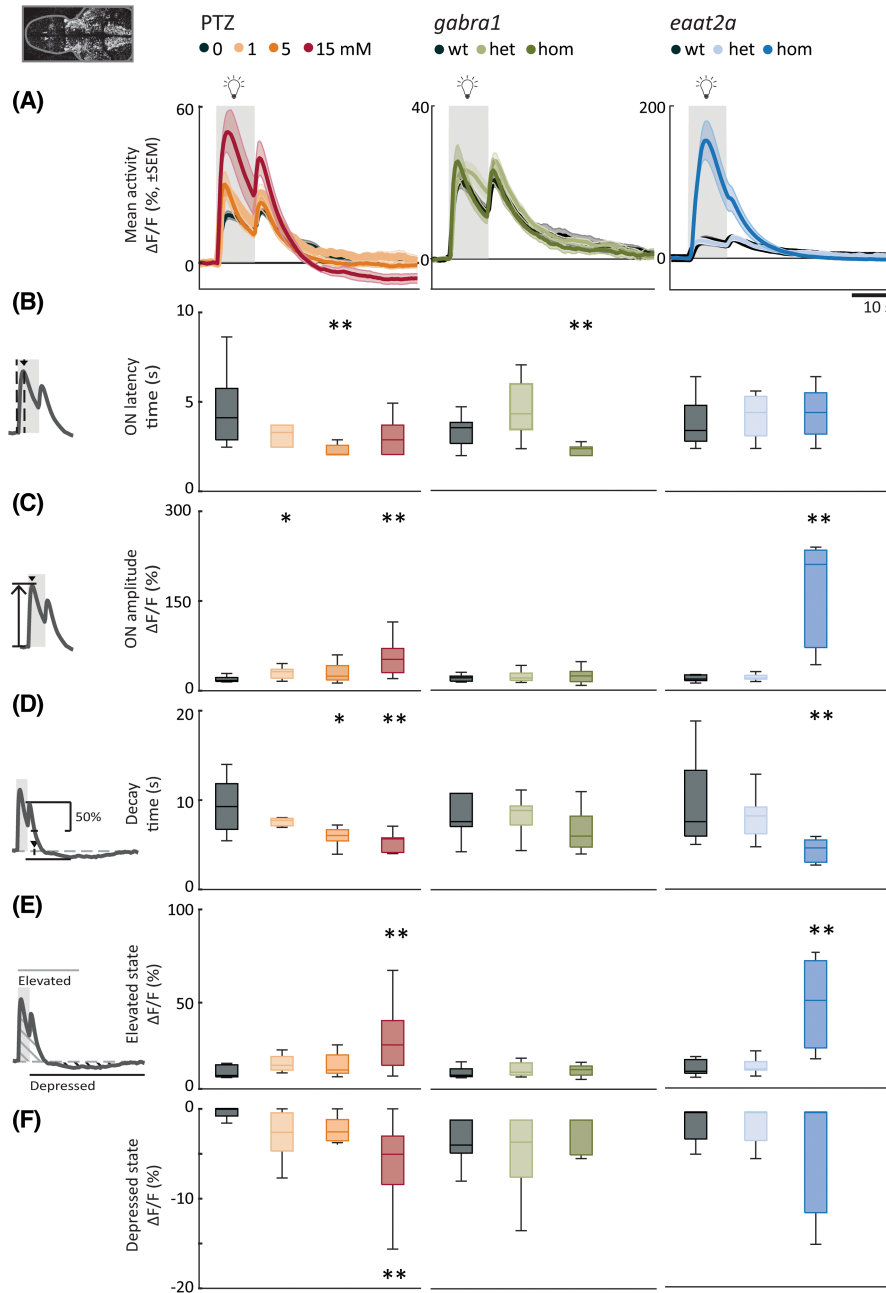


FIGURE 4 Photic stimulation elicits elevated neural responses with fast dynamics and prominent depressed state. (A) Mean neural calcium response (relative change in fluorescence [$\Delta F/F$; %]) to photic stimulation per subgroup averaged across five trials of 5-min interstimulus interval. Gray shaded area indicates photic stimulation. (B) Latency to peak amplitude during 10-s photic stimulation. (C) Peak amplitude during photic stimulation. (D) Time constant for 50% decay of calcium signal from light offset. (E) Elevated state as measured by mean area under the curve above 2 SD from a 1-min baseline (1 min period after light onset). (F) Depressed state as measured by mean area over the curve below 2 SD from a 1-min baseline (first 2 min after light turned off). Total sample size for pentylentetrazole (PTZ) model: control, $n = 8$; $1 \text{ mmol}\cdot\text{L}^{-1}$, $n = 7$; $5 \text{ mmol}\cdot\text{L}^{-1}$, $n = 9$; $15 \text{ mmol}\cdot\text{L}^{-1}$, $n = 10$; for *gabra1* model: wild-type (wt), $n = 9$; heterozygous (het), $n = 13$; homozygous (hom), $n = 9$; for *eaat2a* model: wt, $n = 7$; het, $n = 13$; hom, $n = 11$. For *eaat2a* hom mutants, four of 11 animals had only plateau-like events; hence, seven animals were included in the analyses for this figure. * $p < .05$, ** $p < .01$ by Wilcoxon rank-sum test. Shaded regions of individual colors represent SEM of each group. Boxplots represent median with interquartile ranges; whiskers extend to the most extreme data points that are not outliers

panels). The homozygous *eaat2a* elevated state was more prominent compared to controls, but we did not observe a significant depressed state on a group level (Figure 4E,F, right panels).

Occasionally, we observed photically evoked events leading to a prolonged elevated state without a following depressed state. These responses, which displayed dynamics with an elevated "plateau" phase clearly outlasting the

photic stimulus, were analyzed separately from the briefer "nonplateau" events (Figure S6a,b, S7, Video S4). For the 15-mmol·L⁻¹ PTZ and *gabra1* homozygous mutants, "plateaulike" events were very few, seven of 246 and five of 221 events, respectively (Figure S7). On the contrary, *eaat2a* homozygous animals displayed many plateaulike events (49/265), including more than half of the 5-min ISI events (32/55). The plateau morphology events in *eaat2a* mutants had distinct features, with significantly higher amplitudes and slower dynamics compared to nonplateau events (Figure S6c-f). This suggests that compensatory mechanisms to balance hyperexcitability are not always efficiently recruited during prolonged elevated states in this model.

3.4 | Photically evoked state dynamics are brain region-specific

Next, we asked how the activity of different brain regions is recruited upon photic stimulation. We delineated five brain regions (Figure 5A,F,K, Figure S8a)—the telencephalon (homologous to mammalian cerebrum), thalamus, optic tectum (homologous to superior colliculus in mammals), cerebellum, and brainstem—and analyzed regionwise neural activity. Response dynamics of individual fish (Figure 5B,G,L) and per subgroup (Figure 5C,H,M) appeared to be brain region-dependent. To quantify this, we first detected light-on response peak amplitudes to study latency to maximum response of brain regions (Figure 5D,I,N). We plotted the cumulative proportion of fish in each group that had reached half maximum response across time. A steep rise in the cumulative proportion plot means that the brain region had a short latency to half maximum. Not surprisingly, the neural activity in the optic tectum had the shortest response latency and the strongest amplitude in the PTZ model (Figure 5C-E). Region recruitment was significantly more rapid in the optic tectum compared to all other brain regions except from the thalamus in homozygous *gabra1* animals (Figure 5H-J). Recruitment of the optic tectum was not significantly different from other regions in homozygous *eaat2a* mutants (Figure 5M-O).

We then explored the elevated and depressed states across brain regions (Figure 5B,G,L,C,H,M) by calculating the area under the curve and area over the curve. For the PTZ seizure model, the elevated state was significantly higher for all brain regions except for thalamus in the 15-mmol·L⁻¹ group (Figure S8b, upper panel). The depressed state was significantly more pronounced for all brain regions except for the telencephalon in the 15-mmol·L⁻¹ group (Figure S8b, lower panel), and this state was particularly strong in some individuals

(Figure 5B). In *gabra1* homozygous larvae, both elevated and depressed states were less pronounced compared to PTZ-treated larvae, and not significantly different from controls (Figure S8c). In the *eaat2a* homozygous animals, elevated state was significantly larger for the thalamus, optic tectum, and cerebellum (Figure S8d, upper panel). Although depressed state was similar across subgroups (Figure S8d, lower panel), a few of the *eaat2a* homozygous animals displayed a very distinct depressed state that was seldom observed in controls (Figure 5L).

3.5 | Rapid decay and depression of neural activity following photic stimulation temporally overlaps with slow recruitment of astroglial calcium signals that are enhanced in seizure-prone networks

Our results revealed that seizure-prone networks exhibit an elevated response during the early phase of photic stimulation. We also observed that this hyperexcitable elevated state is often followed by a slow and long-lasting depressed state, which is particularly prominent in the PTZ model. We hypothesized that such long-lasting depressed state might be due to recruitment of astroglial networks that are shown to be important for clearing excess glutamate.^{15,25,37} To test this hypothesis, we measured the astroglial calcium signals during photic stimulation. Astroglial calcium signals displayed strikingly different photic responses (Figure 6B) when compared to the neurons (Figure 6A). The astroglial dynamics were slower in comparison, with a significantly longer latency to maximum amplitude (Figure 6D), and longer decay-time constant (Figure 6E). We also observed that astroglial photic responses were significantly elevated in seizure-prone networks in the presence of PTZ (Figure 6C). Given that the elevated astroglial photic responses are significantly slower and longer lasting when compared to neurons (Figure 6D,E), we asked whether the elevated astroglial responses in seizure-prone networks might temporally correspond to periods when neurons exhibit long-lasting depressed state. To visualize this effect, we calculated the net effect of PTZ on astroglial and neural networks by subtracting the mean calcium response in control fish from the mean response in PTZ-treated fish, and plotted the subtracted signal for astroglial versus neural networks that are temporally aligned thanks to precise photic stimulation (Figure 6F). Strikingly, the subtracted astroglial and neural signals mirrored each other; they were completely anticorrelated (average correlation coefficient of astroglial vs. neural signal = -.5403). Interestingly,

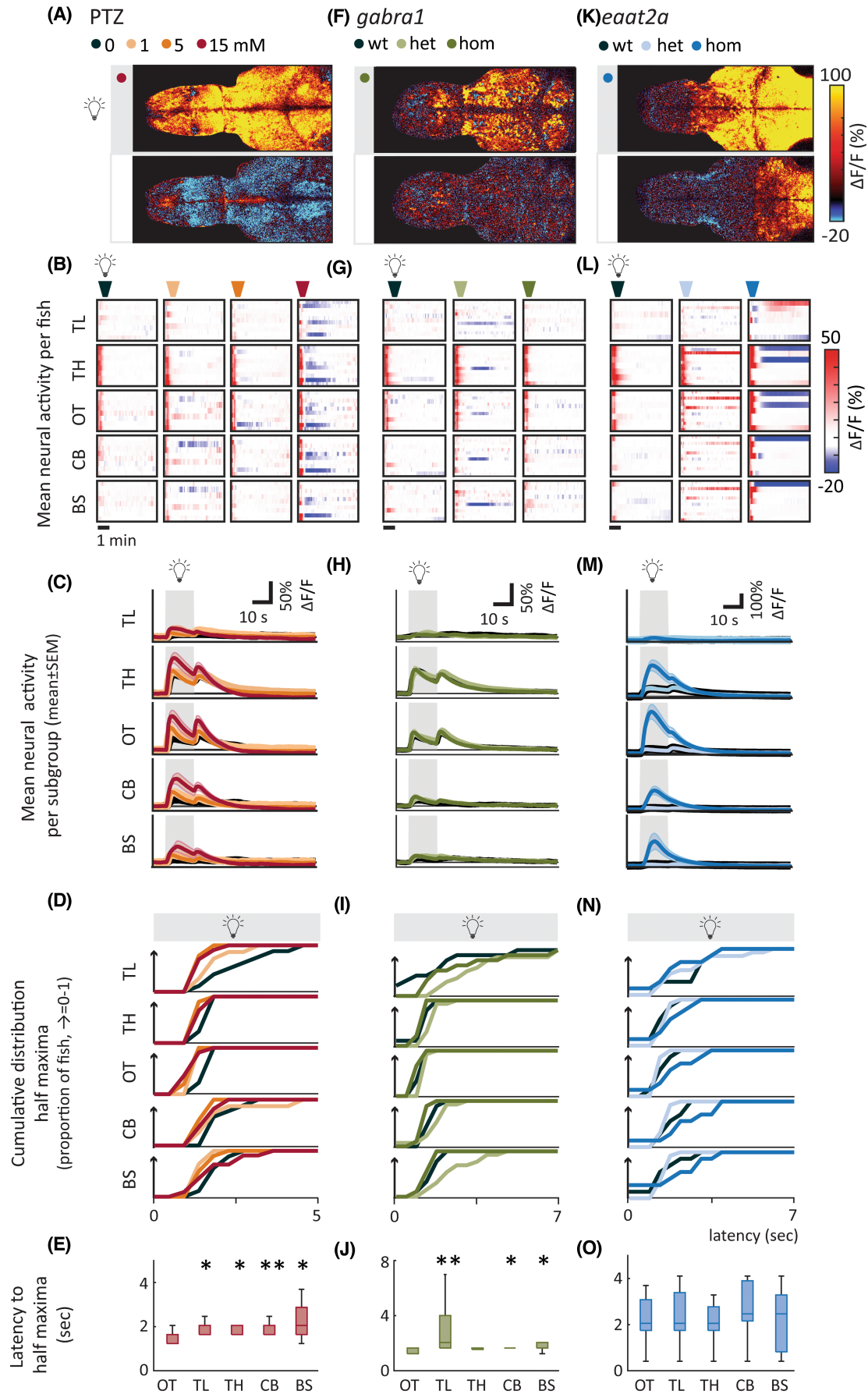


FIGURE 5 Brain regions are differentially recruited upon photic stimulation. (A, F, K) Representative examples of fish during periods when light was turned on and off. Images show mean calcium signals (relative change in fluorescence [$\Delta F/F$; %]) averaged across five trials. Upper panels show a time period starting 5 s after light onset, lower panels from 30 s after light offset. Both show the average activity during a 1.68-s period. (B, G, L) Average calcium signals were extracted from five brain regions: telencephalon (TL), thalamus (TH), optic tectum (OT), cerebellum (CB), and brainstem (BS). Each line in heatmaps represents $\Delta F/F$ of one fish averaged across five trials of 5-min interstimulus interval. (C, H, M) Average activity per subgroup, $\Delta F/F$. (D, I, N) Cumulative distribution of latency to half maxima during photic stimulation. (E, J, O) Latency to half maxima for 15 mmol·L⁻¹ pentylenetetrazole (PTZ; E), homozygous (hom) *gabra1* mutants (J), and hom *eaat2* mutants (O). Latency for optic tectum is compared with the four other brain regions. Total sample size for PTZ model: control, $n = 8$; 1 mmol·L⁻¹, $n = 7$; 5 mmol·L⁻¹, $n = 9$; 15 mmol·L⁻¹, $n = 10$; for *gabra1* model: wild-type (wt), $n = 9$; heterozygous (het), $n = 13$; hom, $n = 9$; for *eaat2a* model: wt, $n = 7$; het, $n = 13$; hom, $n = 11$. For *eaat2a* hom mutants, four of 11 animals had only plateau-like events; hence, seven animals were included in the analyses for this figure. Shaded regions of individual colors represent SEM of each group. * $p < .05$, ** $p < .01$ by Wilcoxon rank-sum test. Boxplots represent median with interquartile ranges; whiskers extend to the most extreme data points that are not outliers

depressed period of neural response coincided with a strong elevation of astroglial activity in PTZ-treated seizure-prone networks. These results suggest that elevated astroglial activity might contribute to the long-lasting depressed state in neural networks.

4 | DISCUSSION

Seizure generation is a dynamic process consisting of both elevated and depressed network states.^{4,5,38} We showed that zebrafish is an efficient model to perform comparative studies on these dynamics in seizure and epilepsy models. First, we demonstrated dose- and model-dependent alterations of spontaneous locomotor and neural activity in line with previous studies.^{22,23,25,26} Exploration of spontaneous locomotion in multiwell assays is an excellent tool for large-scale drug screens.^{22,23} However, lack of an unbiased metric for seizurelike activity and unpredictable occurrence of seizures complicate the interpretation of such studies. We demonstrated how photic stimulation, inspired by human EEG recording paradigms, can enable detailed and comparative investigations of neural and locomotor dynamics of ictogenesis.¹⁸ We showed that our temporally precise photic stimulation approach can enable serial and reliable visualization of neural and astroglial activity. In future experiments, the release of neurotransmitters such as glutamate or GABA may also be examined with a similar approach. Given our results with a confirmed antiseizure medication, VPA, we propose that our photic stimulation assay can be a reliable method to identify the impact of novel antiseizure drug candidates on neural and astroglial excitability and temporal dynamics.

We analyzed photically evoked locomotion during altered excitability states. GABA_A-antagonizing perturbations of PTZ and *gabra1* models led to increased swim velocities upon photic stimulation. *eaat2a* mutants exhibit photically induced locomotor responses, but they

were mostly immobile during rest. In line with previous studies, we observed increased photically induced swimming in *scn1lab*,¹⁸ which was accompanied by an overall reduction of mean swim velocity in the absence of photic stimulation. Previous studies reported an increase in the number of high-speed swim events for *scn1lab* homozygotes compared to their wild-type siblings.³⁹ Nonetheless, some of these studies also reported that mean swim distance (equivalent to swim velocity as we calculated here) is reduced in *scn1lab* mutants.³⁶ Hence, our reduced mean swim velocity measurements in *scn1lab* mutants are consistent with these previous studies. Moreover, the photically evoked change in swim angle was significant in PTZ-treated and *scn1lab* larvae, but not in the *gabra1* and *eaat2a* mutants. This phenotype resembles tonic-clonic-like semiology in zebrafish larvae, consisting of high-speed, swirllike swimming followed by immobility.²²

Photic stimulation elicited an elevated neural activity with larger responses at higher PTZ concentrations and in homozygous *gabra1* and *eaat2a* mutants. The elevated state was most pronounced and recruited fastest in the sensory area optic tectum, which likely is due to triggering of hyperexcitability through the retinal ganglion cell inputs to optic tectum. Nonetheless, we do not see a significant temporal difference of recruitment in *eaat2a* mutants, which may be due to slow and dysfunctional astroglial networks in these animals. Propagation of neural hyperexcitability across the entire brain occurred more rapidly in ictogenic networks, especially in animals treated with the GABA_A antagonist PTZ, breaking down inhibition and facilitating seizure spread.⁸ Strikingly, we demonstrated that this elevated state was often followed by a rapid decay of neural activity and a depressed state. Interestingly, the elevated neural activity correlated with following depression, especially in the PTZ model. Our results highlight a fast switch from elevated to depressed state in ictogenic networks.

What mechanisms might underlie rapid switching between elevated and depressed states? Our results on

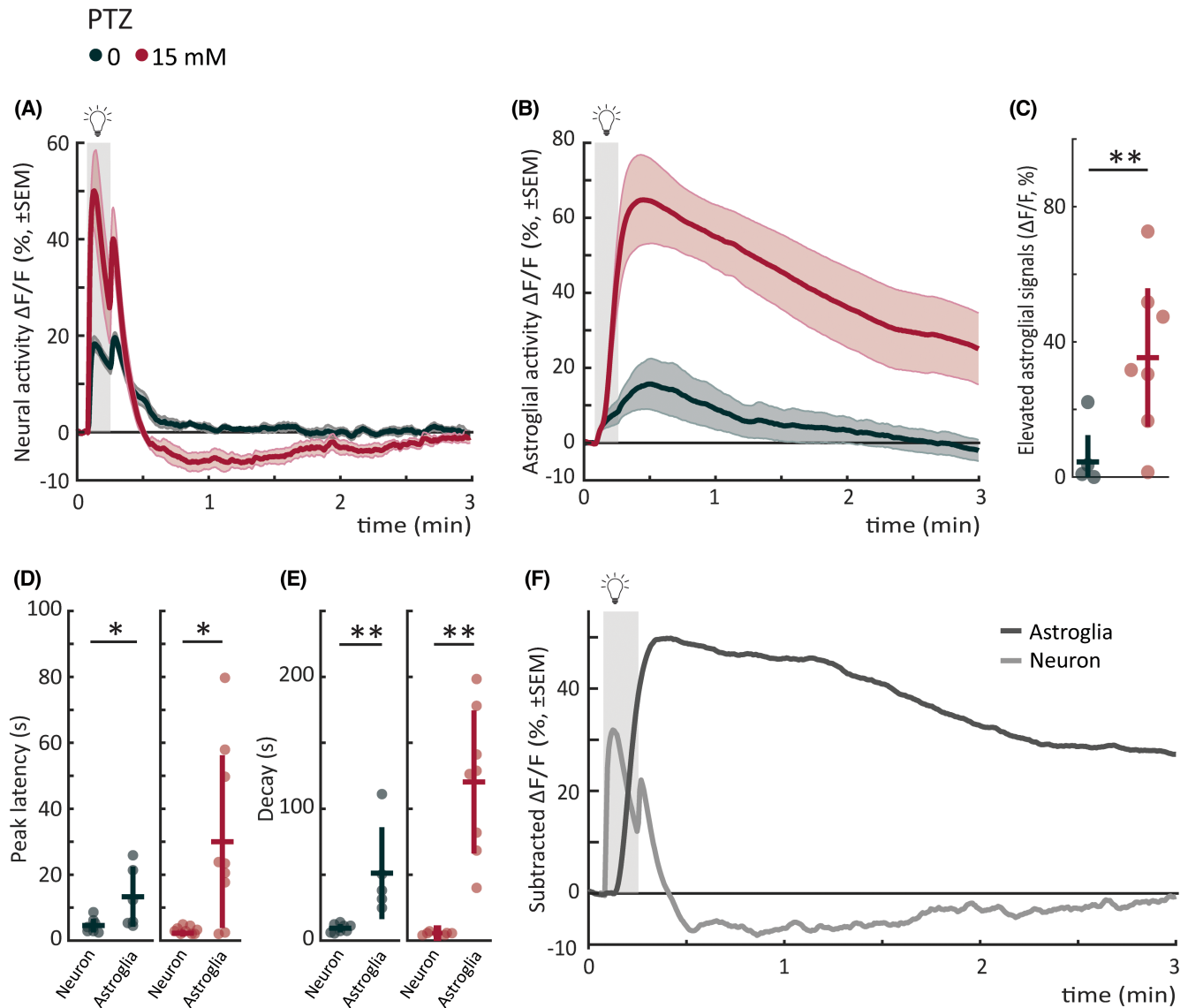


FIGURE 6 Astroglial photic response in seizure-prone networks is slow, elevated, and mirrors neural depressed state. (A) Mean neural calcium response (relative change in fluorescence [$\Delta F/F$; %]) to photic stimulation per subgroup averaged across five trials of 5-min interstimulus interval. Gray shaded area indicates photic stimulation. The same dataset as in Figure 4A pentylenetetrazole (PTZ) trials is replotted for comparison with astroglial signals. (B) Mean astroglial calcium response ($\Delta F/F$) to photic stimulation per subgroup averaged across five trials of 5-min interstimulus interval. Gray shaded area indicates photic stimulation. (C) Elevated astroglial signals as measured by mean area under the curve from a 5-s baseline (5-min period after light onset). (D) Latency to peak amplitude of response during 10-s photic stimulation. Left panel shows neural versus astroglial responses for control; right panel shows the responses for 15 mmol·L⁻¹ PTZ. (E) Time constant for 50% decay of calcium signal from light offset. Left panel shows neural versus astroglial responses for control; right panel shows the responses for 15 mmol·L⁻¹ PTZ. (F) Mean calcium response ($\Delta F/F$) of control fish subtracted from mean response of 15 mmol·L⁻¹ fish for astroglia (dark gray) versus neuron (light gray). Pearson correlation coefficient between average astroglial and neural signal is -0.5403 , calculated from time point of neural light-on response peak until next light stimulus. Gray shaded area indicates photic stimulation. Total sample size for *Tg(GFAP:Gal4);Tg(UAS:GCaMP6s)* "astroglial" recordings: control, $n = 7$; 15 mmol·L⁻¹, $n = 9$; for *Tg(elavl3:GCaMP6s)* "neural" recordings: control, $n = 8$; 15 mmol·L⁻¹, $n = 10$. * $p < .05$, ** $p < .01$ by Wilcoxon rank-sum test. Each data point in scatter plots represents an individual fish. Error bars represent mean \pm SD per subgroup. Shaded regions of individual colors represent SEM of each group.

astroglial calcium signals might shed light on this question. We observed that upon photic stimulation, astroglia exhibit slow and long-lasting calcium signals compared to neurons. Moreover, we showed that PTZ-treated seizure-prone networks exhibit highly elevated astroglial calcium

signals, temporally overlapping with the period when neural calcium signals exhibit fast decay and strong depression. Hence, our observations suggest that astroglial networks are involved in this fast decay and depression phase, likely through the action of astroglial glutamate

transporters, which we have investigated in an earlier study.²⁵ We would like to highlight that this observation and temporal matching of neural and astroglial calcium signals would not have been possible without photic stimulation.

It is known that elevated (or hyperexcitable) and hypersynchronous brain activity arises during epileptic seizures. Although depressed states are observed in epilepsy patients and animal models, they are less understood.^{38,40} Landmark studies in hippocampal and cortical slices revealed the paroxysmal depolarizing shift (PDS) phenomenon.^{41–43} These electrophysiological recordings were performed in GABA_A-antagonist models and demonstrated remarkable dynamics. First, the membrane potential enters a plateau phase with a train of action potentials, followed by an extended afterhyperpolarization aborting the elevated state. The PDS is hypothesized as the cellular correlate of interictal spikes observed in EEG in patients.^{41–43} The PDS dynamics are considered to be shaped by ion fluxes through voltage-gated Na⁺, K⁺, and Ca²⁺ channels.⁴² Moreover, astroglia–neuron interactions^{15,25} and effects of neuromodulators like acetylcholine⁴ may play important roles. It has been proposed that such long-lasting plateau phases might be related to seizure propagation.⁴⁴ We observed elevated to depressed state transitions upon photic stimulation in our models, resembling PDS. Moreover, in some animals, we even observed long-lasting, elevated plateau-like events outlasting the stimuli. The roles of the depressed (or hyperpolarized) state are enigmatic. PDS studies suggest that the depressed states may protect against seizure propagation,^{43,45} and cell death through glutamate excitotoxicity.⁴⁶ Timing, location, and degree of depressed states may play important roles. The relevance of PDS for human EEG dynamics has yet mostly been inferred from in vitro models. Zebrafish may serve as an in vivo model to explore the mechanisms of this PDS-like phenomenon across the entire brain.

Although several features of neural dynamics were generalizable across zebrafish seizure and epilepsy models, we also demonstrated differences related to the underlying pathophysiology. Dose-dependent augmentation of elevated state occurred upon treatment with the GABA_A antagonist PTZ. However, genetic perturbation of GABA_A receptor in *gabra1* mutants did, surprisingly, produce less pronounced elevation. This weaker phenotype in *gabra1* mutants might be due to previously observed alterations in expression levels of several other genes including the GABA transporters, and machinery for GABA_A receptor trafficking, leading to genetic compensation in these mutants.²⁶ Importantly, a previous study reported photically induced seizures in *gabra1* mutant juvenile zebrafish,²⁶ whereas we examined larval zebrafish, which are better suited for high-throughput screens. In humans, monogenic

gabra1 disorders display a broad phenotypic spectrum ranging from juvenile myoclonic epilepsy to severe epileptic encephalopathies, where spontaneous and photic reflex seizures may develop already from early childhood.⁴⁷ In line with the human phenotype, we detect subtle signs of altered brain excitability already in early stage zebrafish larvae, using photic stimulation. Instead, *eaat2a* mutants produced a different response. This model, with decreased astroglial uptake of glutamate, showed particularly strong “light-on” neural responses, as previously reported.²⁵ Contrary to the strong photically evoked responses in homozygous *eaat2a* larvae, their spontaneous neural activity was significantly less pronounced compared to wild-type. One important mechanism underlying this hypoactive state might be reduced glutamate availability due to depletion of presynaptic glutamate pool after seizures and impaired glutamate recycling in *eaat2a* mutants.²⁵

Photic stimulation resulted in increased neural and locomotor responses, in line with tonic–clonic seizure-like behavior, in zebrafish larvae. This response may be comparable to photoparoxysmal responses (PPRs) on human EEG. Intermittent photic stimulation (IPS) is performed in routine diagnostic EEGs to detect epileptiform activity.¹⁶ PPRs are seen in several epilepsies including juvenile myoclonic epilepsy.^{16,19,48} In some patients, epileptic seizures are related to PPRs. EEG responses that outlast the IPS trains are considered to have a strong association with epilepsy.¹⁶ In our zebrafish seizure models, the frequently observed short-lasting elevated photic responses may relate to self-limited PPRs in human patients, whereas the long-lasting plateau type responses may be comparable to self-sustaining PPRs.^{49,50}

Photosensitivity has previously been studied in both humans and several animal models of epilepsy (Table 1). The two most extensively studied models are the primate *Papio papio* baboon^{53–58,65} and the Fayoumi chicken.^{60–63,65} Recently, novel models of Rhodesian ridgeback dog⁵⁹ and a nonvertebrate *Drosophila*⁶⁴ model were introduced. In our zebrafish models, photic stimulation induced the earliest and strongest neural response in midbrain structures, which is in line with a proposed mesencephalic seizure initiator in the Fayoumi chicken.⁶⁰ Intriguingly, elegant studies on Fayoumi chimeras highlighted the importance of interactions between cortical and subcortical structures in nonmammalian species without a neocortex,^{60,66} similar to previous studies in zebrafish.^{15,25} Photic reflex seizures were shown to be initiated most typically in cortical areas in primates; in temporo-occipital regions in humans,^{20,51,52} whereas in the baboon a frontal origin was suggested.^{53,54} The seizure semiology in the *Papio papio* baboon, Fayoumi chicken, and our zebrafish models is considered to be generalized.^{53–58,60–63}

TABLE 1 Photosensitivity in humans and animal models

Species	Semiology	Brain region involvement	Photic stimulation	Etiology
Human ^{20,51,52}	Myoclonic seizures, absence seizures, GTCs, focal seizures	PPR generated predominantly in parieto-occipital regions	IPS, 15–20 Hz most ictogenic	Genetic component; candidate susceptibility genes (e.g., <i>GABRA1</i> , <i>CHD2</i>)
<i>Papio papio</i> baboon ^{53–58}	Myoclonic seizures, GTCs	Initiation in primary motor cortices, with secondary activation of prefrontal cortices and thalamus	IPS, 20–25 Hz most ictogenic	Unknown; proposed genetic
Rhodesian ridgeback dog ⁵⁹	Myoclonic seizures, GTCs	Generalized 4–5-Hz spike-and-wave pattern with predominantly frontocentral maximum	IPS, PPR at 3–17 Hz in 4 of 6 tested animals	Genetic (DIRAS family GTPase 1, <i>DIRAS1</i>)
Fayoumi chicken ^{60–63}	Neck myoclonia, usually developing to a GTC-like seizure	Proposed mesencephalic “seizure generator”; studies in chimeras imply that both prosencephalon and mesencephalon are needed for generalized seizures	IPS, ~14 Hz most ictogenic	Genetic (SV2A)
Zebrafish (present study) ^{17,25,26}	GTC-like behavior (high-speed swirllike behavior followed by immobility)	Early activation of midbrain structures (in particular optic tectum, homologous to mammalian superior colliculus), may generalize	Nonflickering light stimuli	Genetic (<i>gabral1</i> , ²⁶ <i>eat2a</i> , ²⁵ <i>scn11ab1</i>) Pharmacological
Fruit fly ⁶⁴	Motor seizures	No information on initiation site; only whole-brain activity analyzed	IPS, 60-Hz paradigm	Genetic (ceramide phosphoethanolamine synthase, <i>cpes</i>)

Abbreviations: GTC, generalized tonic-clonic; GTCs, GTC seizure; GTPase, guanosine triphosphatase; IPS, intermittent photic stimulation; PPR, photoparoxysmal response.

Typically, application of IPS is used in human patients and animal models (Table 1). We used 10-s-long light stimuli in our zebrafish models, which elicited the most reproducible locomotor response. In human patients, flash frequencies between 15 and 20 Hz have been shown to be the most ictogenic. Low-frequency visual evoked potentials (VEPs) are mostly limited to testing the functional integrity of the visual system,⁶⁷ and are less explored in epilepsy. Patients with photosensitive occipital lobe epilepsy were reported to show increased VEP amplitudes consistent with hypersynchrony^{68,69} and abnormal latencies.⁶⁸ VEPs may be a valuable tool to investigate brain excitability, especially sub-seizure-threshold dynamics. We also propose that photic stimulation could be explored more in rodent epilepsy models, where invasive methods like electrical stimulation are commonly used to induce seizures.^{17,70} Further studies on low-frequency photic stimulation might reveal potential biomarkers in epilepsy and other disorders of altered excitability.

Our findings on depressed network states and seizure propagation may have clear relevance for clinical practice. Traditionally, antiseizure medications are considered to exert their effects by reducing hyperexcitability. More recently, different drugs were shown to display differential effects on seizure propagation.⁷¹ We argue that investigating mechanisms underlying elevated and depressed states in seizure models have great potential. Precise temporally controlled photic stimulation is a powerful tool both as a medium- to high-throughput screening tool, and for detailed studies on underlying mechanisms. Our protocol allowed us to study astroglial and neural networks in parallel experiments, and showed that both these networks are highly involved especially during the depressed network state.²⁵ An improved understanding of the interplay between elevated and depressed excitability states might suggest tailored therapies targeting these states at the network level and should be studied further.

5 | CONCLUSIONS

In a side-by-side comparison of seizure and epilepsy models, we show that features of spontaneous locomotor and neural activity vary across models. Instead, an elevated photic response with faster dynamics is well preserved across all models. Intriguingly, we observed that elevated photic response is often followed by a fast decay and depressed state. Our findings highlight that both hyperactivity and hypoactivity are prominent features of seizure-prone networks. We propose that photic stimulation may be a useful tool to investigate altered brain excitability and dynamics in vertebrate seizure and epilepsy

models. This powerful zebrafish platform enables efficient evaluation of novel models, and may be well suited for both testing novel therapeutical approaches and dissecting the underlying physiology of seizure generation.

AUTHOR CONTRIBUTIONS

Conceptualization: Ahmed Jamali, Nathalie Jurisch-Yaksi, Emre Yaksi. Methodology: Ahmed Jamali, Sverre Myren-Svelstad, Percival P. D'gama, Nathalie Jurisch-Yaksi, Emre Yaksi. Data analysis: Sverre Myren-Svelstad, Ahmed Jamali. Software: Sverre Myren-Svelstad, Ahmed Jamali, Anna M. Ostenrath, Aytac Kadir Mutlu. Providing reagents and data: Adriana L. Hotz, Stephan C. F. Neuhaus. Investigation: all authors. Writing: Sverre Myren-Svelstad, Ahmed Jamali, Nathalie Jurisch-Yaksi, Emre Yaksi. Review & editing: all authors. Funding acquisition: Sverre Myren-Svelstad, Nathalie Jurisch-Yaksi, Emre Yaksi. Supervision: Nathalie Jurisch-Yaksi, Emre Yaksi.

ACKNOWLEDGMENTS

We thank M. Ahrens (HHMI, Janelia Farm, USA) for the *Tg(elavl3:GCaMP6s)* transgenic line, P. de Witte (KU Leuven, Belgium) for the *scn1lab* mutant line, and É. Samarut (University of Montreal, Canada) for the *gabral* mutant line; S. Eggen, V. Nguyen, A. M. Nygaard, and our fish facility support team for technical assistance; and T. Sand, P. M. Omland, and E. Brodtkorb (St Olav's University Hospital and Norwegian University of Science and Technology) and the Yaksi laboratory members for stimulating discussions. This work was funded by a Liaison Committee for Education, Research, and Innovation in Central Norway (Samarbeidsorganet) grant (S.M.-S., N.J.-Y., E.Y.); the Medical Student's Research Program, Norwegian University of Science and Technology (A.J., S.S.O., H.H.H.); an RSO grant, Norwegian University of Science and Technology (A.M.O.); RCN FRIPRO research grants 314189 (N.J.-Y.), 239973 (E.Y.), and 314212 (E.Y.); and ERC starting grant 335561 (E.Y.). Work in the E.Y. laboratory is funded by the Kavli Institute for Systems Neuroscience at Norwegian University of Science and Technology.

CONFLICT OF INTEREST

None of the authors has any conflict of interest to disclose.

ORCID

Sverre Myren-Svelstad  <https://orcid.org/0000-0003-4258-8028>

Ahmed Jamali  <https://orcid.org/0000-0002-1929-0779>

Sunniva S. Ophus  <https://orcid.org/0000-0002-2889-9682>


Percival P. D'gama  <https://orcid.org/0000-0002-7145-0557>


Anna M. Ostenrath  <https://orcid.org/0000-0001-8344-4528>

Aytac Kadir Mutlu  <https://orcid.org/0000-0003-1318-6425>

Helene Homme Hoffshagen  <https://orcid.org/0000-0003-4526-9807>

Adriana L. Hotz  <https://orcid.org/0000-0003-1992-7829>

Stephan C. F. Neuhaus  <https://orcid.org/0000-0002-9615-480X>

Nathalie Jurisch-Yaksi  <https://orcid.org/0000-0002-8767-6120>

Emre Yaksi  <https://orcid.org/0000-0003-3761-0235>

REFERENCES

- Fisher RS, van Emde BW, Blume W, Elger C, Genton P, Lee P, et al. Epileptic seizures and epilepsy: definitions proposed by the International League Against Epilepsy (ILAE) and the International Bureau for Epilepsy (IBE). *Epilepsia*. 2005;46(4):470–2.
- Yaksi E, Jamali A, Diaz Verdugo C, Jurisch-Yaksi N. Past, present and future of zebrafish in epilepsy research. *FEBS J*. 2021;288:7243–55.
- Sills GJ, Rogawski MA. Mechanisms of action of currently used antiseizure drugs. *Neuropharmacology*. 2020;168:107966.
- Motelow JE, Li W, Zhan Q, Mishra AM, Sachdev RN, Liu G, et al. Decreased subcortical cholinergic arousal in focal seizures. *Neuron*. 2015;85(3):561–72.
- Blumenfeld H. Impaired consciousness in epilepsy. *Lancet Neurol*. 2012;11(9):814–26.
- Crunelli V, Lőrincz ML, McCafferty C, Lambert RC, Leresche N, Di Giovanni G, et al. Clinical and experimental insight into pathophysiology, comorbidity and therapy of absence seizures. *Brain*. 2020;143(8):2341–68.
- Pottkämper JCM, Hofmeijer J, van Waarde JA, van Putten M. The postictal state—what do we know? *Epilepsia*. 2020;61(6):1045–61.
- Paz JT, Huguenard JR. Microcircuits and their interactions in epilepsy: is the focus out of focus? *Nat Neurosci*. 2015;18(3):351–9.
- Jirsa VK, Stacey WC, Quilichini PP, Ivanov AI, Bernard C. On the nature of seizure dynamics. *Brain*. 2014;137(8):2210–30.
- Stam CJ. Modern network science of neurological disorders. *Nat Rev Neurosci*. 2014;15(10):683–95.
- van Diessen E, Diederer SJ, Braun KP, Jansen FE, Stam CJ. Functional and structural brain networks in epilepsy: what have we learned? *Epilepsia*. 2013;54(11):1855–65.
- Burrows DRW, Samarut É, Liu J, Baraban SC, Richardson MP, Meyer MP, et al. Imaging epilepsy in larval zebrafish. *Eur J Paediatr Neurol*. 2020;24:70–80.
- Rosch R, Burrows DRW, Jones LB, Peters CH, Ruben P, Samarut É. Functional genomics of epilepsy and associated neurodevelopmental disorders using simple animal models: from genes, molecules to brain networks. *Front Cell Neurosci*. 2019;13:556.
- Rosch RE, Hunter PR, Baldeweg T, Friston KJ, Meyer MP. Calcium imaging and dynamic causal modelling reveal brain-wide changes in effective connectivity and synaptic dynamics during epileptic seizures. *PLoS Comput Biol*. 2018;14(8):e1006375.
- Diaz Verdugo C, Myren-Svelstad S, Aydin E, Van Hoeymissen E, Deneubourg C, Vanderhaeghe S, et al. Glia-neuron interactions underlie state transitions to generalized seizures. *Nat Commun*. 2019;10(1):3830.
- Kasteleijn-Nolst Trenité D, Rubboli G, Hirsch E, Martins da Silva A, Seri S, Wilkins A, et al. Methodology of photic stimulation revisited: updated European algorithm for visual stimulation in the EEG laboratory. *Epilepsia*. 2012;53(1):16–24.
- Eimon PM, Ghannad-Rezaie M, De Rienzo G, Allalou A, Wu Y, Gao M, et al. Brain activity patterns in high-throughput electrophysiology screen predict both drug efficacies and side effects. *Nat Commun*. 2018;9(1):219.
- Ghannad-Rezaie M, Eimon PM, Wu Y, Yanik MF. Engineering brain activity patterns by neuromodulator polytherapy for treatment of disorders. *Nat Commun*. 2019;10(1):2620.
- Poleon S, Szaflarski JP. Photosensitivity in generalized epilepsies. *Epilepsy Behav*. 2017;68:225–33.
- Fisher RS, Acharya JN, Baumer FM, French JA, Parisi P, Solodar JH, et al. Visually sensitive seizures: an updated review by the Epilepsy Foundation. *Epilepsia*. 2022;63(4):739–68.
- Baraban SC, Dinday MT, Hortopan GA. Drug screening in *Scn1a* zebrafish mutant identifies clemizole as a potential Dravet syndrome treatment. *Nat Commun*. 2013;4(1):2410.
- Baraban SC, Taylor MR, Castro PA, Baier H. Pentylentetrazole induced changes in zebrafish behavior, neural activity and c-fos expression. *Neuroscience*. 2005;131(3):759–68.
- Afrikanova T, Serruys AS, Buenafe OE, Clinckers R, Smolders I, de Witte PA, et al. Validation of the zebrafish pentylentetrazol seizure model: locomotor versus electrographic responses to antiepileptic drugs. *PLoS One*. 2013;8(1):e54166.
- Tiraboschi E, Martina S, van der Ent W, Grzyb K, Gawel K, Cordero-Maldonado ML, et al. New insights into the early mechanisms of epileptogenesis in a zebrafish model of Dravet syndrome. *Epilepsia*. 2020;61(3):549–60.
- Hotz AL, Jamali A, Rieser NN, Niklaus S, Aydin E, Myren-Svelstad S, et al. Loss of glutamate transporter *eaat2a* leads to aberrant neuronal excitability, recurrent epileptic seizures, and basal hypoactivity. *Glia*. 2022;70(1):196–214.
- Samarut É, Swaminathan A, Riché R, Liao M, Hassan-Abdi R, Renault S, et al. γ -Aminobutyric acid receptor alpha 1 subunit loss of function causes genetic generalized epilepsy by impairing inhibitory network neurodevelopment. *Epilepsia*. 2018;59(11):2061–74.
- McKeown KA, Moreno R, Hall VL, Ribera AB, Downes GB. Disruption of *Eaat2b*, a glutamate transporter, results in abnormal motor behaviors in developing zebrafish. *Dev Biol*. 2012;362(2):162–71.
- Vladimirov N, Mu Y, Kawashima T, Bennett DV, Yang CT, Looger LL, et al. Light-sheet functional imaging in fictively behaving zebrafish. *Nat Methods*. 2014;11(9):883–4.
- Muto A, Lal P, Ailani D, Abe G, Itoh M, Kawakami K. Activation of the hypothalamic feeding centre upon visual prey detection. *Nat Commun*. 2017;8(1):15029.
- Turrini L, Fornetto C, Marchetto G, Müllenbroich MC, Tiso N, Vettori A, et al. Optical mapping of neuronal activity during seizures in zebrafish. *Sci Rep*. 2017;7(1):3025.
- Reiten I, Uslu FE, Fore S, Pelgrims R, Ringers C, Diaz Verdugo C, et al. Motile-cilia-mediated flow improves sensitivity and

- temporal resolution of olfactory computations. *Curr Biol*. 2017;27(2):166–74.
32. Fore S, Acuña-Hinrichsen F, Mutlu KA, Bartoszek EM, Serneels B, Faturos NG, et al. Functional properties of habenular neurons are determined by developmental stage and sequential neurogenesis. *Sci Adv*. 2020;6(36):eaaz3173.
 33. Olstad EW, Ringers C, Hansen JN, Wens A, Brandt C, Wachten D, et al. Ciliary beating compartmentalizes cerebrospinal fluid flow in the brain and regulates ventricular development. *Curr Biol*. 2019;29(2):229–41.e6.
 34. Jetti SK, Vendrell-Llopis N, Yaksi E. Spontaneous activity governs olfactory representations in spatially organized habenular microcircuits. *Curr Biol*. 2014;24:434–9.
 35. Kroll F, Powell GT, Ghosh M, Gestri G, Antinucci P, Hearn TJ, et al. A simple and effective F0 knockout method for rapid screening of behaviour and other complex phenotypes. *Elife*. 2021;10:e59683.
 36. Grone BP, Qu T, Baraban SC. Behavioral comorbidities and drug treatments in a zebrafish *scn1lab* model of Dravet syndrome. *eNeuro*. 2017;4(4):ENEURO.0066-17.2017.
 37. Heuser K, Enger R. Astrocytic Ca²⁺ signaling in epilepsy. *Front Cell Neurosci*. 2021;15(257):695380.
 38. Keller CJ, Truccolo W, Gale JT, Eskandar E, Thesen T, Carlson C, et al. Heterogeneous neuronal firing patterns during interictal epileptiform discharges in the human cortex. *Brain*. 2010;133(Pt 6):1668–81.
 39. Griffin A, Carpenter C, Liu J, Paterno R, Grone B, Hamling K, et al. Phenotypic analysis of catastrophic childhood epilepsy genes. *Comm Biol*. 2021;4(1):680.
 40. Blumenfeld H. What is a seizure network? Long-range network consequences of focal seizures. *Adv Exp Med Biol*. 2014;813:63–70.
 41. Matsumoto H, Marsan CA. Cortical cellular phenomena in experimental epilepsy: interictal manifestations. *Exp Neurol*. 1964;9:286–304.
 42. Ayala GF, Dichter M, Gumnit RJ, Matsumoto H, Spencer WA. Genesis of epileptic interictal spikes. New knowledge of cortical feedback systems suggests a neurophysiological explanation of brief paroxysms. *Brain Res*. 1973;52:1–17.
 43. Kubista H, Boehm S, Hotka M. The paroxysmal depolarization shift: reconsidering its role in epilepsy, epileptogenesis and beyond. *Int J Mol Sci*. 2019;20(3):577.
 44. Tryba AK, Merricks EM, Lee S, Pham T, Cho S Jr, Nordii DR, et al. Role of paroxysmal depolarization in focal seizure activity. *J Neurophysiol*. 2019;122(5):1861–73.
 45. Schevon CA, Weiss SA, McKhann G Jr, Goodman RR, Yuste R, Emerson RG, et al. Evidence of an inhibitory restraint of seizure activity in humans. *Nat Commun*. 2012;3:1060.
 46. Sarlo GL, Holton KF. Brain concentrations of glutamate and GABA in human epilepsy: a review. *Seizure*. 2021;91:213–27.
 47. Johannesen K, Marini C, Pfeffer S, Møller RS, Dorn T, Niturad CE, et al. Phenotypic spectrum of GABRA1: from generalized epilepsies to severe epileptic encephalopathies. *Neurology*. 2016;87(11):1140–51.
 48. Baykan B, Wolf P. Juvenile myoclonic epilepsy as a spectrum disorder: a focused review. *Seizure*. 2017;49:36–41.
 49. Puglia JF, Brenner RP, Soso MJ. Relationship between prolonged and self-limited photoparoxysmal responses and seizure incidence: study and review. *J Clin Neurophysiol*. 1992;9(1):137–44.
 50. Jayakar P, Chiappa KH. Clinical correlations of photoparoxysmal responses. *Electroencephalogr Clin Neurophysiol*. 1990;75(3):251–4.
 51. Kasteleijn-Nolst Trenité DG. Photosensitivity in epilepsy. Electrophysiological and clinical correlates. *Acta Neurol Scand Suppl*. 1989;125:3–149.
 52. Takasaka Y, Takamatsu K, Nakagawara M. Anterior-posterior relationships of EEG in photosensitive subjects: coherence and cross-phase-spectral analysis. *Jpn J Psychiatry Neurol*. 1989;43(4):651–63.
 53. Fischer-Williams M, Poncet M, Riche D, Naquet R. Light-induced epilepsy in the baboon, *Papio papio*: cortical and depth recordings. *Electroencephalogr Clin Neurophysiol*. 1968;25(6):557–69.
 54. Silva-Barrat C, Ménini C, Bryère P, Naquet R. Multiunitary activity analysis of cortical and subcortical structures in paroxysmal discharges and grand mal seizures in photosensitive baboons. *Electroencephalogr Clin Neurophysiol*. 1986;64(5):455–68.
 55. Menini C, Naquet R. Myoclonia. From the myoclonia of *Papio papio* to various human myoclonias [in French]. *Rev Neurol (Paris)*. 1986;142(1):3–28.
 56. Szabó C, González DA, Koneru S. Semiology of spontaneous generalized tonic-clonic seizures in the epileptic baboon. *Epilepsia Open*. 2020;5(2):213–9.
 57. Szabó CA, Narayana S, Kochunov PV, Franklin C, Knape K, Davis MD, et al. PET imaging in the photosensitive baboon: case-controlled study. *Epilepsia*. 2007;48(2):245–53.
 58. Naquet R, Catier J, Menini C. Neurophysiology of photoinduced epilepsy in *Papio papio*. *Adv Neurol*. 1975;10:107–18.
 59. Wielaender F, Sarviaho R, James F, Hytönen MK, Cortez MA, Kluger G, et al. Generalized myoclonic epilepsy with photosensitivity in juvenile dogs caused by a defective DIRAS family GTPase 1. *Proc Natl Acad Sci U S A*. 2017;114(10):2669–74.
 60. Guy N, Teillet MA, Schuler B, Gal L, la Salle G, Le Douarin N, et al. Pattern of electroencephalographic activity during light induced seizures in genetic epileptic chicken and brain chimeras. *Neurosci Lett*. 1992;145(1):55–8.
 61. Crichlow EC, Crawford RD. Epileptiform seizures in domestic fowl. II. Intermittent light stimulation and the electroencephalogram. *Can J Physiol Pharmacol*. 1974;52(3):424–9.
 62. Douaud M, Feve K, Pituello F, Gourichon D, Boitard S, Leguern E, et al. Epilepsy caused by an abnormal alternative splicing with dosage effect of the SV2A gene in a chicken model. *PLoS One*. 2011;6(10):e26932.
 63. Crawford RD. Epileptiform seizures in domestic fowl. *J Hered*. 1970;61(5):185–8.
 64. Kunduri G, Turner-Evans D, Konya Y, Izumi Y, Nagashima K, Lockett S, et al. Defective cortex glia plasma membrane structure underlies light-induced epilepsy in *cpe* mutants. *Proc Natl Acad Sci U S A*. 2018;115(38):E8919–28.
 65. Martins da Silva A, Leal B. Photosensitivity and epilepsy: current concepts and perspectives—a narrative review. *Seizure*. 2017;50:209–18.
 66. Naquet R, Batini C. Varieties of photosensitivity in man ("plain" and progressive myoclonus epilepsies), in baboon and in fowl. In: Zifkin B, Inoue Y, Wolf P, editors. *Reflex epilepsies: progress in understanding*. Esher, UK: John Libbey; 2004:15–26.

67. Odom JV, Bach M, Brigell M, Holder GE, McCulloch DL, Mizota A, et al. ISCEV standard for clinical visual evoked potentials (2016 update). *Doc Ophthalmol.* 2016;133(1):1–9.
68. Porciatti V, Bonanni P, Fiorentini A, Guerrini R. Lack of cortical contrast gain control in human photosensitive epilepsy. *Nat Neurosci.* 2000;3(3):259–63.
69. Brinciotti M, Mittica A, Matricardi M. Characteristics of visual evoked potentials related to the electro-clinical expression of reflex seizures in photosensitive patients with idiopathic occipital lobe epilepsy. *Epilepsy Res.* 2020;164:106345.
70. Bertram E. The relevance of kindling for human epilepsy. *Epilepsia.* 2007;48(Suppl 2):65–74.
71. Khateb M, Bosak N, Herskovitz M. The effect of anti-seizure medications on the propagation of epileptic activity: a review. *Front Neurol.* 2021;12(683):674182.

SUPPORTING INFORMATION

Additional supporting information can be found online in the Supporting Information section at the end of this article.

How to cite this article: Myren-Svelstad S, Jamali A, Ophus SS, D’gama PP, Ostenrath AM & Mutlu AK et al. Elevated photic response is followed by a rapid decay and depressed state in ictogenic networks. *Epilepsia.* 2022;63:2543–2560. <https://doi.org/10.1111/epi.17380>